J Mater Sci (2007) 42:7363–7374
DOI 10.1007/s10853-007-1555-4

# Frequency and temperature dependence of electrical properties of barium and gadolinium substituted $SrBi_2Nb_2O_9$ ceramics

**Konapala Sambasiva Rao · Dasari Madhava Prasad · Prayaga Murali Krishna · B. Hima Bindu · K. Suneetha**

Received: 20 October 2006 / Accepted: 26 January 2007 / Published online: 15 May 2007


**Abstract** Barium strontium gadolinium bismuth niobate ($Ba_{0.1}Sr_{0.81}Gd_{0.06}Bi_2Nb_2O_9$, BSGBN) ceramics were prepared by using the conventional solid-state reaction method. The dielectric permittivity, modulus and impedance spectroscopy studies on BSGBN were investigated in the frequency range, 45 Hz–5 MHz and in the temperature range from room temperature (RT) to 570 °C. The dielectric anomaly with a broad peak was observed at 470 °C. Simultaneous substitution of $Ba^{2+}$ and $Gd^{3+}$ increases the transition temperature of $SrBi_2Nb_2O_9$ (SBN) from 392 to 470 °C. XRD studies in BSGBN revealed an orthorhombic structure with lattice parameters $a$ = 5.4959 Å, $b/a$ = 1.000, $c$ = 25.0954 Å. Impedance and modulus plots were used as tools to analyse the sample behaviour as a function of frequency. Cole-Cole plots showed a non-Debye relaxation. Also, dc and ac conductivity measurements were performed on BSGBN. The electric impedance which describes the dielectric relaxation behaviour is fitted to the Kohlrausch exponential function. Near the phase transition temperature, a stretched exponential parameter $\beta$ indicating the degree of distribution of the relaxation time has a small value.

## Introduction

The layered pervoskite materials described by Aurivillius are named after him as Aurivillius compounds [1–3]. Electric fatigue due to repeated switching in ferroelectric materials and devices has attracted much interest. Many researchers have managed to apply conductive oxide electrodes to improve the fatigue endurance of ferroelectric materials and devices [4–9]. Another method was to search for naturally antifatigue ferroelectric materials. Layered structure pervoskite including $SrBi_2Ta_2O_9$ (SBT) or $SrBi_2Nb_2O_9$ (SBN) was proven to be the ideal candidates for fabrication of non-volatile ferroelectric random access memory (NVFeRAM), which could endure $10^{12}$ electric cycles [10–13]. However, compared to the traditional PZT solid solution system their ferroelectric properties were not favourable due to small saturated and remanent polarization, large coercive fields.

The chemical formula of Aurivillius compounds is $(Bi_2O_2)^{2+}$ $(A_{x-1}B_xO_{3x+1})^{2-}$, where A represents the 12-fold coordinated cations with low valances in the pervoskite sublattice such as mono-, di- or trivalent ions or a mixture of them; B is a combination of cations denotes the octahedral site with high valances like $Fe^{3+}$, $Ti^{4+}$, $Nb^{5+}$, $Ta^{5+}$, $W^{6+}$; $x$ is the number of octahedral layers in the pervoskite block between the rock-salt type $(Bi_2O_2)^{2+}$ layers along the $c$-axis. Strontium bismuth niobate is one of the family of layer-pervoskite ferroelectrics ($SrBi_2Nb_2O_9$, $x$ = 2). The materials in this class have been found to have wide spread applications in a variety of ferroelectric-based devices [10, 14]. The Aurivillius-type ferroelectric phases with high $T_C$ are very much interesting as bulk materials for devices such as ultrasonic sensors, accelerometers [15], ceramic transducers [16, 17] etc to work at high temperatures. Furthermore, BLSF ceramics have been considered to be promising materials as lead-free electroceramics from the viewpoint of environmental protection [18, 19]. Figure 1 shows the lattice structure of $ABi_2B_2O_9$.

Subba Rao reported that the Curie temperature decreases when the size of A site cations in BLSFs increases [20–22].

K. Sambasiva Rao (✉) · D. Madhava Prasad · P. Murali Krishna · B. Hima Bindu · K. Suneetha
Centre for Piezoelectric Transducer Materials, Department of Physics, Andhra University, Visakhapatnam 530 003, India
e-mail: konapala@sify.com

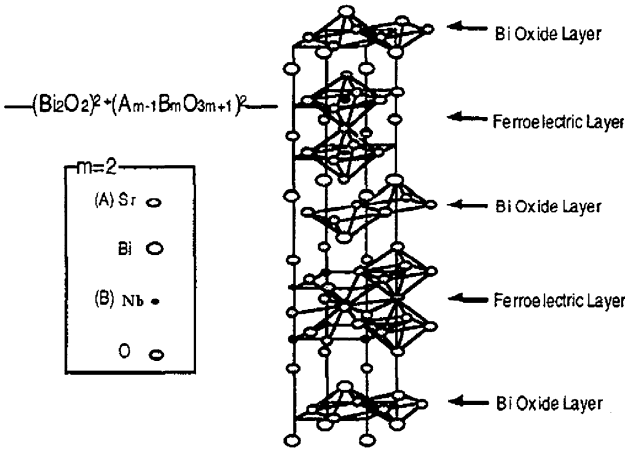


**Fig. 1** Lattice structure of $ABi_2B_2O_9$-type bismuth layer-structured ferroeletric material

Newnham et al. reported that the structure of 10 at% of $Sr^{2+}$ substituted by $Ba^{2+}$ in SBT with lower Curie temperature and reduced distortions in the pervoskite units [23]. Millan et at. [24–26] studied the substitution of $Bi^{3+}$ in the bismuth oxide layer by other cations, like $Pb^{2+}$, $Sb^{3+}$ and $Te^{4+}$. It was found that the SBN structure could be preserved by such substitution, and the dielectric properties vary with the substitution of alternative cations. There are many reports on the substitution of A site ions, $Sr^{2+}$, in the pervoskite unit cells, by $Bi^{3+}$ or $Ba^{2+}$ [27, 28].

In general, such substitutions resulted in higher polarization; however, no thorough explanation was given [27, 28]. Forbess et al. [29] have also studied the influence of $La^{3+}$ and $Ca^{2+}$ doping on the dielectric properties of SBN ferroelectric ceramics. It was found that doping with $La^{3+}$ and $Ca^{2+}$ resulted in an appreciable increase in the Curie points and noticeable decrease in the dc conductivity. There are also many research reports in the open literature [30–33] on solid solutions based on the SBTN systems. However, few studies can be found on the improvement of ferroelectric properties of the layered pervoskite ferroelectrics through substitution of the B site ions ($Nb^{5+}$ or $Ta^{5+}$) with other alternative cations [34, 35].

In all ferroelectrics, in general, the study of electrical conductivity is very important since the associated physical properties like piezoelectricity, pyroelectricity and also strategy for poling are dependent on the order and nature of conductivity in these materials.

The ac impedance method is a promising non-destructive technique for analysing ferroelectric and piezoelectrics. The electric conductivity studies indicate the nature of dominant constituents or charge species involved in the conduction on application of an electric field. Transport and relaxation properties can be described at higher temperatures with reference to inter particle interaction.

Venkataraman et al. [36, 37] reported that the dielectric constant data obtained on undoped and vanadium-doped SBN ceramics, at various frequencies and temperatures of interest. An attempt has been made to rationalize the dielectric behaviour in terms of Jonscher's model. However, dielectric and impedance spectroscopic studies have not been found in literature on the simultaneous substitution of Barium and Gadolinium in SBN to understand the transport properties.

The present article, reports the preparation, structure, and frequency dependence of the dielectric constant, impedance, modulus and conductivity as a function of temperature.

## Experimental

Polycrystalline composition of $Ba_{0.1}Sr_{0.81}Gd_{0.06}Bi_2Nb_2O_6$ (henceforth abbreviated as BSGBN) was prepared by a high-temperature solid-state reaction technique by taking analar grade carbonates and oxides: $BaCO_3$, $SrCO_3$, $Gd_2O_3$, $Bi_2O_3$ and $Nb_2O_5$ (all Aldrich Chemicals, with purity >99.5%) in desired quantity. These ingredients were thoroughly mixed in wet atmosphere (methanol) in an agate mortar for 6 h, and then dried by slow evaporation. The mixture was calcined in air for 4 h at 900 °C with intermediate grinding and heating stages in order to obtain homogenous powder. The formation of the monophasic compound of BSGBN was confirmed via X-ray powder diffraction (XRD) using Cu Kα radiation. The calcined powder was used to make disc pellets of diameter 10 mm and thickness 1–2 mm using a hydraulic press at a pressure of 450 MPa. Polyvinyl alcohol (PVA) was used as a binder to bring the particles closure. The pressed pellets were sintered in air at 1,160 °C for 60 min. The densities of the sintered pellets were determined by the liquid displacement/Archimedes method [38]. The pellets were polished to make both faces flat and parallel. For electrical characterizations, the pellet's flat surfaces were painted with high-purity air-drying conducting silver paste and heated at 600 °C for 30 min. The electrical and dielectric properties of the sample have been carried out by a computer controlled HIOKI LCR Hitester model 3532 over a wide frequency range (45 Hz–5 MHz) and in the temperature range (35–590 °C).

## Results and discussion

### XRD

Figure 2 shows the X-ray diffractogram of BSGBN. It has been indexed on using a standard computer program

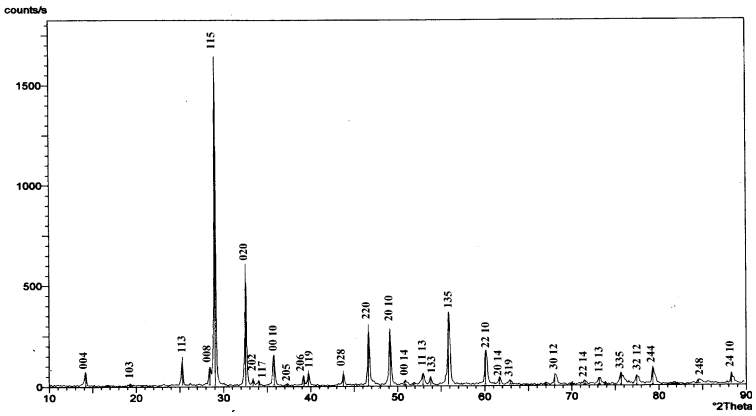


**Fig. 2** X-ray diffractogram of BSGBN

(POWD) [39]. The characteristic value of 100% intensity peak in SBN has been found at $2\theta = 29.4144°$ for which indexed *hkl* values are 115. In the present BSGBN, the 100% intensity peak observed at $2\theta = 29.03129°$ for which the *d*-spacing is 3.0732 Å, the assigned *hkl* values are 115. The shift in $2\theta$ value to 29.03129° is due to the substitution of Barium and Gadolinium in SBN.

The sample was indexed to be orthorhombic with lattice parameters $a = 5.4959$ Å, $b/a = 1.000$, $c = 25.0954$ Å. The reported [40] lattice constants in SBN were $a = 5.506$ Å, $b/a = 1.000$ and $c = 25.05$ Å. Substitution of Ba and La slightly decreases the value of '*a*' and increases '*c*' to that of SBN. The value of density, 7.13 gm/cm$^3$ has been found in BSGBN.

However, simultaneous substitution of Ba and Gd has influenced the lattice parameters without altering basic crystal structure. The density of the sample was 96% of the theoretical density. The theoretical density ($d_{the}$), experimental density ($d_{exp}$), orthorhombic distortion *b*/*a*, porosity and % of density values in BSGBN are given in Table 1.

## Dielectric

### *Temperature-dependent real (ε′) and imaginary (ε″) part of the dielectric constant*

Figure 3 shows the temperature dependence of the real ($\varepsilon'$) and imaginary ($\varepsilon''$) part of the dielectric constant at 0.5, 1, 10 and 20 kHz. The room temperature dielectric constant ($\varepsilon_{RT}'$) at 1 kHz is 117. The dielectric maxima corresponding temperature observed to be 470 °C at 1 kHz, which is the transition temperature ($T_C$) of the material. Dielectric constant versus temperature at 1 kHz in SBN has been depicted in the inset of Fig. 3a, ferroelectric transition

**Table 1** Lattice parameters of BSGBN

| Composition | Lattice parameters (Å) | Orthorhombic distortion (*b*/*a*) | Density (g/cm$^3$) | | % density | Porosity |
|---|---|---|---|---|---|---|
| | | | X-ray | Exp | | |
| BSGBN | $a = 5.4959$<br>$c = 25.0954$ | 1.000 | 7.42 | 7.13 | 96 | 0.04 |

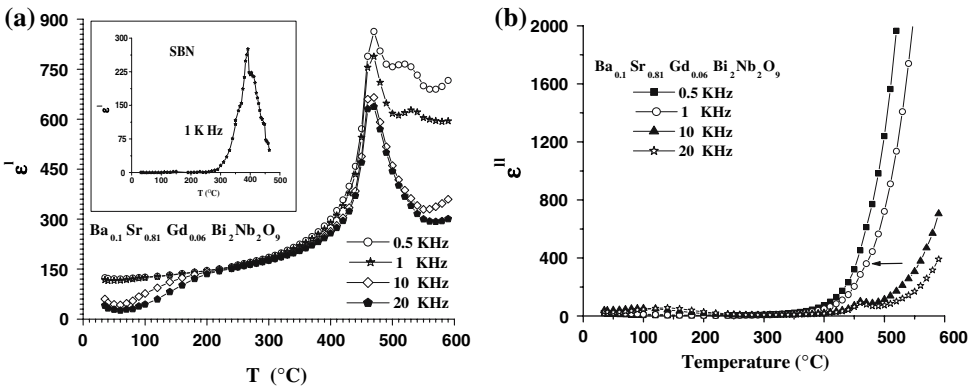


**Fig. 3** (**a**) Temperature dependence of ε′ at various frequencies. (**b**) Temperature dependence of ε″ at different frequencies

temperature of SBN has been found at 392 °C. The value of dielectric constant at $T_C$ ($\varepsilon_{TC}'$) is 788. The value of $T_C$ in SBN has been reported as 418, 420 and 440 °C by different authors [20, 29, 41]. Now in the present system, simultaneous substitution of 10% $Ba^{2+}$ and 6% $Gd^{3+}$ also increases the value of $T_C$, 392 °C of SBN to 470 °C. However, no shift in $T_C$ value has been observed at different frequencies indicating BSGBN belongs to traditional ferroelectrics but not relaxor. The permittivity data at 1 kHz was fitted to the Curie–Weiss law in para-region:

$$\varepsilon' = C/(T - T_C) \quad (1)$$

The Curie constant ($K$), $1.1 \times 10^5$ °C has been observed and the value is in good agreement with the value $0.82 \times 10^5$ reported by Jianjun Liu et al. [42]. The values of $\varepsilon_{RT}^{1}$, $T$ °C, $\varepsilon_{TC}^{1}$ room temperature conductivity $\sigma_{RT}$, and Curie constant ($K$) are given in Table 2.

It is obvious from Fig. 3b, $\varepsilon''$ versus temperature, a change in slope has been observed at a particular temperature, 470 °C corresponds to the $T_C$ value and independent of frequency. Further, $\varepsilon''$ found to be approximately independent of frequency and temperature up to 350 °C.

*Frequency dependence of the dielectric constants $\varepsilon'$ and $\varepsilon''$*

Figure 4 shows frequency dependence of $\varepsilon'$ and $\varepsilon''$ at different temperatures. The real part of the dielectric constant, which implies the charge storage, has a strong dispersion in the low-frequency region. The imaginary part of the dielectric constant, which is dominated by the conduction of mobile charge, has nearly a single slope. From Fig. 4 both the values of $\varepsilon'$ and $\varepsilon''$ almost start at approximately 420 at 45 Hz and 400 °C. As the temperature increases to 450 °C, $\varepsilon'$ increases to 1,000, whereas, $\varepsilon''$ increases to above 2,000. Also, they intersect at a frequency, 0.2 kHz. Further, increase in temperature both $\varepsilon'$ and $\varepsilon''$ values are increased and intersection frequency shifts towards the higher frequency side. This massive rise in $\varepsilon''$ indicates the mechanism of polarization is not unique in the low- and high-frequency region. The low-frequency dispersion is

**Table 2** Dielectric data

| Composition | $\varepsilon_{RT}^{1}$ (1 kHz) | $T_C$ (°C) | $\varepsilon_{TC}^{1}$ (1 kHz) | Curie constant, $K$ ($\times 10^5$) | $\sigma_{RT}$ ($\times 10^{-8}$/cm) |
|---|---|---|---|---|---|
| BSGBN | 117 | 470 | 788 | 1.1 | 1.2 |

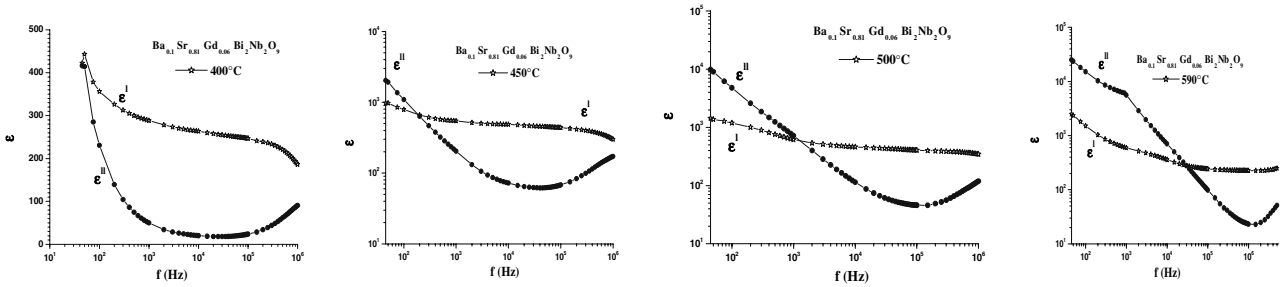


**Fig. 4** The variation of real and imaginary dielectric constant as a function of frequency at several temperatures

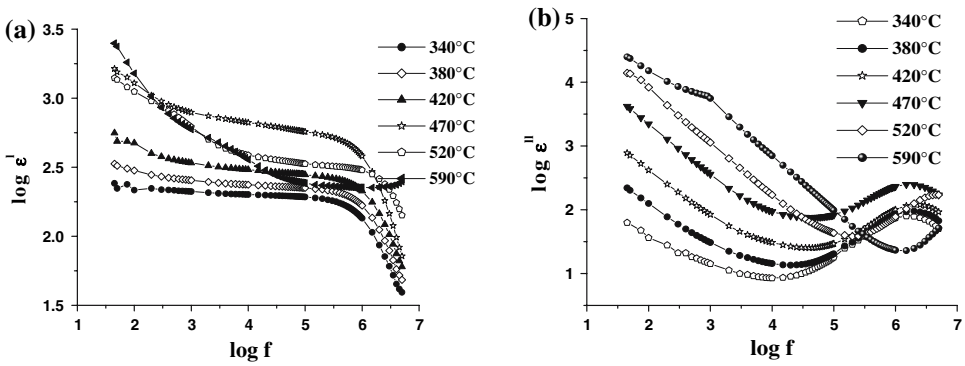


**Fig. 5** (**a**) Frequency dependency of $\varepsilon'$ on log–log scale at different temperatures. (**b**) Frequency dependency of $\varepsilon''$ on log–log scale at different temperatures

observed and is understood that the conducting process is due to ion hopping.

The frequency dependence of $\varepsilon'$ and $\varepsilon''$ on a log–log scale at different temperatures are shown in Fig. 5a and b. Both $\varepsilon'$ and $\varepsilon''$ shows strong dispersion at low frequencies. It is attributed to the low-frequency space charge accumulation effect. Such strong dispersions in both the components of the complex dielectric constant appear to be a common feature in ferroelectrics associated with non-negligible ionic conductivity and is referred to as the low-frequency dielectric dispersion (LFDD) [43, 44]. Detailed studies of this phenomenon were carried by Jonscher et al. [45].

The dispersion in $\varepsilon''$ is stronger than that in the real part implying that it is influenced by dc conductivity. The low-frequency slope of the curve log $\varepsilon''$ versus log $f$ is close to –1 indicating the predominance of the dc conduction in this frequency region.

Figure 6a shows the variation of the real part of the ac conductivity as a function of frequency at a few elevated temperatures. It indicates the existence of low-frequency independent plateau-like region ($\sigma_{dc}$) and subsequently the conductivity increases with increase in frequency, varying approximately as a power of frequency ($\omega^n$) (where $n$ is a function of temperature as well as frequency) at all the temperatures. However, the trend of the curve does not change with temperature; only the onset of the dispersion is shifted to higher frequencies as the temperature is increased. This observation is on line with that reported in the literature for $0.3Na_2O_{0.7}B_2O_3$ glass samples by Roling et al. [46].

The interaction between the charge carriers participating in the polarization process is characterized by the parameter n. A unit value of n implies a Debye case, and it is attainable [47] at very low temperatures. However, as the temperature increases, the interaction increases, leading to a decrease in $n$. The value of n calculated from the high-frequency region decreases as the temperature increases and attains a minimum near $T_C$ and subsequently it increases with further increase in temperature. The observed minimum, 0.923 at $T_C$ implies the strong interaction between the charge carriers and the lattice. Figure 6b shows the variation of critical exponent n with temperature. The Arrhenius plot derived from the conductivity values at different temperatures at 100 Hz is shown as the inset in Fig. 6a. The activation energy calculated from this plot is 0.84 eV and it is close to the ionic conducting resulting from the mobile oxygen ion vacancies and found to be in agreement with the earlier reports [70].

*Dielectric dispersion relations and interpretation of the experimental results*

The complex dielectric constant as a function of the frequency $\omega$ in accordance with the Jonscher's power law is given by the following expression:

$$\varepsilon^* = \varepsilon' - i\varepsilon'' = \varepsilon_\infty + \sigma/i\varepsilon_0\omega + (a(T)/\varepsilon_0)\left(i\omega^{n(T)-1}\right) \quad (2)$$

where $\varepsilon_\infty$ is the 'high-frequency' value of the dielectric constant, $n(T)$ is the temperature-dependent exponent and $a(T)$ determines the strength of the polarizability arising from the universal mechanism in question. $\varepsilon'$ and $\varepsilon''$ are given by the following relations

$$\varepsilon' = \varepsilon_\infty + \sin(n(T)\pi/2)\omega^{n(T)-1}\ (a(T)/\varepsilon_0) \quad (3)$$

$$\varepsilon'' = \sigma/\varepsilon_0\omega + \cos(n(T)\pi/2)\omega^{n(T)-1}\ (a(T)/\varepsilon_0) \quad (4)$$

where the first term in Eq. 3 determines the lattice response and that in Eq. 4 corresponds to the dc conduction part, while the second term in both the equations reflects the charge carrier contribution to the dielectric constant. The temperature and frequency dependencies of the dielectric constant $\varepsilon'$ (Figs. 2a and 4) could be explained by Eq. 3.

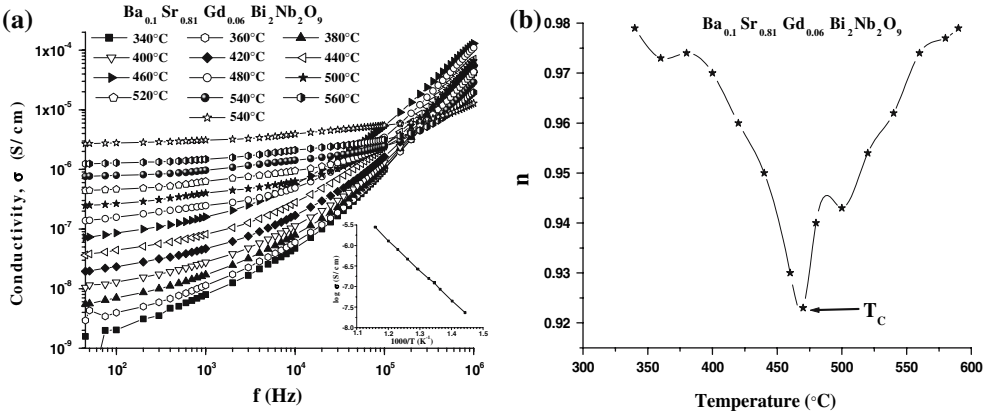


**Fig. 6** (**a**) ac conductivity versus frequency at several temperatures. (**b**) Variation of critical exponent $n(T)$ with temperature showing a minimum at $T_C$

The charge carrier term $(\sin(n(T)\pi/2)\omega^{n(T)-1}\ (a(T)/\varepsilon_0))$ dominates at low frequency and $\varepsilon_\infty$ is negligible. Therefore, for a constant n, Eq. 3 yields a straight line with a slope equal to $n-1$ in the double logarithmic plot of $\varepsilon'$ and frequency. At high frequencies the charge carriers fail to respond to the external field, therefore the measured dielectric constant is due to the contribution from the lattice polarization. This accounts for a linear decrease in the low-frequency region and a frequency-independent plateau region at high frequencies (Fig. 5a). As $A(T)$ $(a(T))$ increases with increase in temperature [48], the charge carrier term becomes more and more prominent at high temperatures, thereby resulting in the low-frequency dielectric dispersion. An anomalously strong dispersion of $\varepsilon'$ near $T_C$ suggests the coupling between the charge carriers and the lattice [49].

The behaviour of $\varepsilon''$ could be explained by Eq. 4. Careful analysis of Fig. 5b indicates the existence of two slopes corresponding to –1 in the low-frequency region and $-(1-n)$ in the high-frequency region. As the dc conductivity term increases with increase in temperature, the second term in Eq. 4 is totally over-shadowed by the first term. So at low frequencies and high temperatures, the dc conductivity term dominates and yields a slope of –1, which indeed is consistent with the data shown in Fig. 5b. Figure 7 shows the temperature dependence of the pre-factor $A(T)$ showing a peak with a value –9.30 at $T_C$. The pre-factor $A(T)$ which determines the strength of polarizability exhibits a peak at $T_C$ [43].

## Impedance and modulus spectroscopic studies

Complex impedance analysis is a well-known and powerful tool which has been effectively used for probing into the dielectric materials. This analysis enables one to resolve the contributions of various processes such as the electrode effects, bulk effects and the interfaces viz the grain boundaries etc in the frequency domain. When the relaxation times of various processes differ as a consequence of different capacitive components, the complex impedance representation is made use of. In the complex impedance plot (Cole-Cole; $Z'$ versus $Z''$ plotted in a linear scale), depending on the relative values of their relaxation times, they gives rise to three semicircular arcs. Generally, the arc at the high-frequency end refers to bulk electrical conduction, the intermediate arc corresponds to the conduction by the grain boundaries and the arc at the low-frequency end arises from electrode processes. Each of these semicircles could be represented by a single RC combination. A depressed semicircle whose centre lies below the real axis suggests the departure from ideal Debye behaviour. The semicircle passes through a maximum at a frequency, $f_0$ (relaxation frequency) and satisfies the condition:

$$\omega\tau = 1$$

On the other hand complex modulus and permittivity plane plots are used to represent the response of dielectric system [50].

From the real part $(Z')$ and imaginary part $(Z'')$ of complex impedance $(Z^*)$, real and imaginary part of modulus $(M', M'')$ and dielectric constant $(\varepsilon', \varepsilon'')$ were obtained using the immitance relations [51]:

$$M' = \omega C_0 Z''$$

$$M'' = \omega C_0 Z'$$

$$\varepsilon' = Z''/(\omega C_0 |Z|^2)$$

Complex impedance plane plots of $Z'$ versus $Z''$ are useful for determining the dominant resistance of a sample but are insensitive to the smaller values of resistances. Similarly, complex modulus plots are useful in determining the smallest capacitances. Sinclair and West [52] suggested the combined usage of impedance and modulus spectroscopic plots to rationalize the dielectric properties. The peak heights are proportional to $R$ for the $Z''$ versus frequency plots and $C^{-1}$ for the $M''$ peak. However, the power of combined usage of both impedance and modulus spectroscopies is that the $Z''$ plot highlights the phenomenon of largest resistances where as $M''$ picks up those of the smallest capacitances [53].

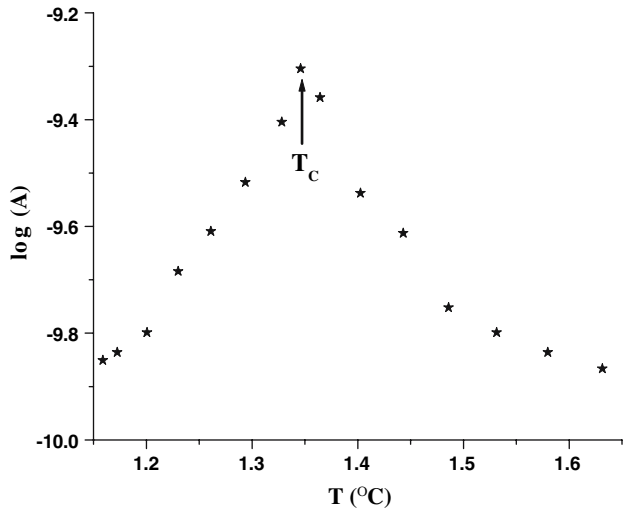


**Fig. 7** The temperature dependence of the pre-factor $A(T)$ showing a peak at $T_C$

*Impedance characterization*

In polycrystalline ceramics sometimes it is not possible to identify each individual component by its own arc in an impedance and modulus spectrum because of the proximity of the time constants. In this case the centre of the experimental arcs in the spectrum is frequently displaced below the real axis because of the presence of different elements in the material-electrode system [51]. These are distorted by the other relaxations whose means constant are within two orders of magnitude or less of that for the arc under consideration. Thus, the spectra show overlapping arcs. Even so, the impedance spectrum in conjunction with a careful characterization can be used to glean information that is otherwise inaccessible—for example, regarding the conductivities of individual phases.

Figure 8 shows Cole-Cole plots of impedance in BSGBN at different temperature in frequency range (45 Hz–5 MHz). At lower temperature (<440 °C) there is a linear response. This trend indicates the insulating behaviour in the sample. As the temperature increases above 440 °C the linear response gradually changes to semicircle in nature. At and above 440 °C the single arc found in the sample can be resolved into two semicircles with overlapping. These semicircles can be represented by the equivalent two parallel RC elements which are in series. Two RC equivalent circuits were assigned to this response shown in Fig. 9.

Frequency dependent $Z'$ and $Z''$, and its corresponding organd diagram are shown at 520°C in Fig. 10. Organd diagram allows us to determine the bulk ohmic resistance as a function of temperature and there by temperature dependence of the conductivity. As the frequency increases $Z^{I}$ decreases and $Z^{II}$ increases, at a particular frequency $Z^{I}$ intersects on $Z^{II}$ response, indicating the existence of

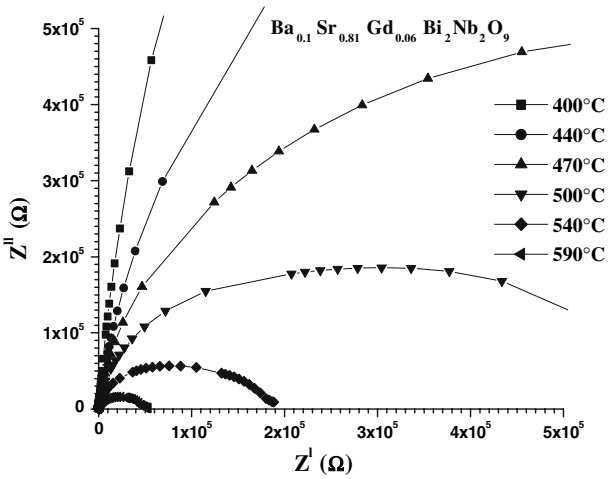


**Fig. 8** Complex impedance plots at different temperatures

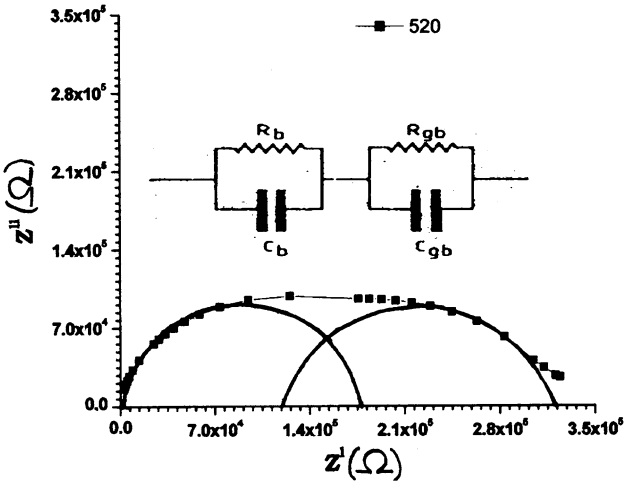


**Fig. 9** Equivalent circuit at 520 °C

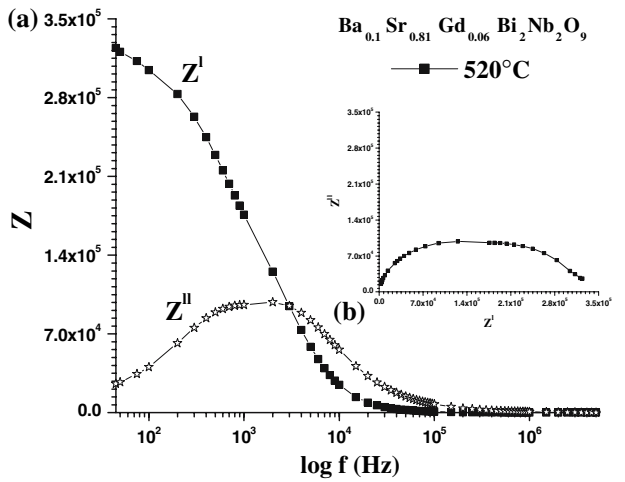


**Fig. 10** (**a**) Frequency dependent of $Z'$ and $Z''$. (**b**) Corresponding argand diagram

impedance relaxation and above 100 kHz values of $Z^{I}$ and $Z^{II}$ merges.

In Fig. 11a, for the temperature range studied, the grain resistance is more compared with grain boundary. From Fig. 11b, the grain capacitance is low compared with grain boundary. At 420 °C, $C_g$ = 1.15 nF and $C_{gb}$ = 0.25 nF and $C_g$ shows a linear decrease where as $C_{gb}$ varies non-linearly. Variation of grain and grain boundary relaxation time with temperature is shown in Fig. 11c. Further, at all the measured temperature scale, grain boundary relaxation time is more than the grain relaxation time with a small difference in their magnitudes.

Variation of grain, grain boundary resistance and relaxation time shows Arrhenius behaviour. Grain and grain boundary conduction activation energy ($E_g$ and $E_{gb}$) grain and grain boundary relaxation activation energy $\varepsilon_g$

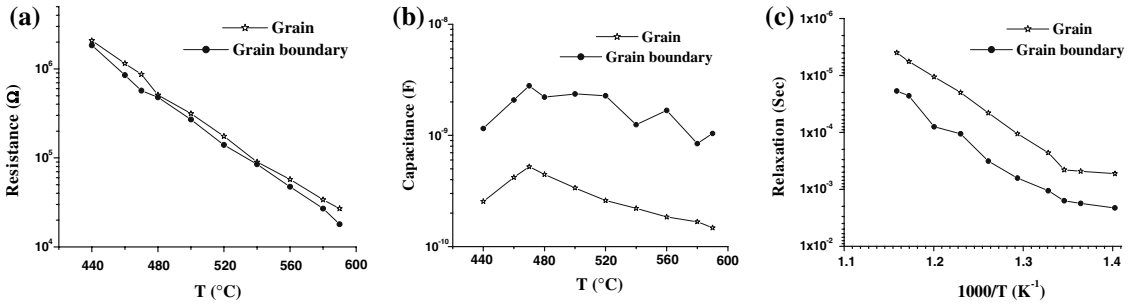


**Fig. 11** (**a**–**c**) Variation of grain, grain boundary (**a**) resistance (**b**) capacitance (**c**) relaxation with temperature

**Table 3** Activation energy values (eV) for conduction ($E$) and relaxation ($\varepsilon$) for grain (b) and grain boundary (gb)

| Temperature range (°C) | Grain conduction activation energy, $E_b$ (eV) | Grain boundary conduction activation energy, $E_{gb}$ (eV) | Temperature range (°C) | Grain relaxation activation energy, $\varepsilon_b$ (eV) | Grain boundary relaxation activation energy, $\varepsilon_{gb}$ (eV) |
|---|---|---|---|---|---|
| 430–470 | 0.63 | 0.76 | 430–470 | 0.21 | 0.25 |
| 480–530 | 0.62 | 0.68 | 500–590 | 0.86 | 1.00 |
| 540–590 | 0.57 | 0.74 | | | |

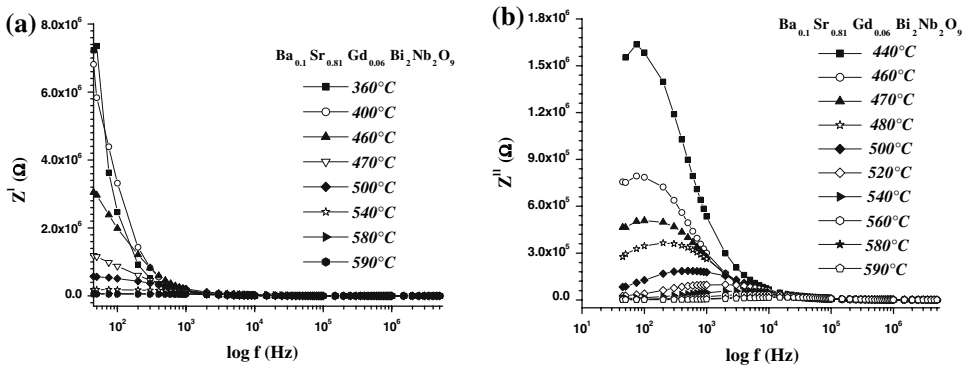


**Fig. 12** (**a**) $Z'$ (Ω) versus frequency (Hz) and (**b**) $Z''$ (Ω) versus frequency (Hz) at various temperatures

and $\varepsilon_{gb}$ have been evaluated and are given in Table 3. Activation energies obtained for conduction through grain and grain boundary indicates the conduction takes place mainly through grain boundaries rather than grains.

Figure 12a presents $Z'$ versus frequency. $Z'$ has higher values at lower frequencies and decreases up to 10 kHz and attains a constant value beyond. The coincidence of impedance ($Z'$) at higher frequencies at all temperatures indicates a possible release of space charge [54]. The frequency dependent $Z''$ is shown in Fig. 12b. $Z''$ showed a peak at a certain frequency in the high-temperature regime (440–590 °C) and the magnitude of $Z''$ decreased with increase of temperature indicating increase in loss in the material. The peak occurs at and above 440 °C and shifts to higher frequencies with increase in temperature, indicating the relaxation in the system. The relaxation frequency can be obtained either from the plot of $Z''$ against frequency or semicircles from the Nyquist plots. The peak broadening on increasing temperature, suggests the presence of temperature dependent relaxation process in the compound [55]. The relaxation process may be due to the presence of immobile species at low temperature and defects at high temperature.

Figure 13a shows the normalized imaginary parts, $Z''/Z''_{max}$, of the impedance as a function of frequency at several temperatures. It seems that high temperature triggers another relaxation process. The $Z''/Z''_{max}$ parameter exhibits a peak with a slightly asymmetric degree at each temperature especially at higher temperatures. At the peak, the relaxation is defined by the condition:

$$\omega_m \tau_m = 1 \tag{9}$$

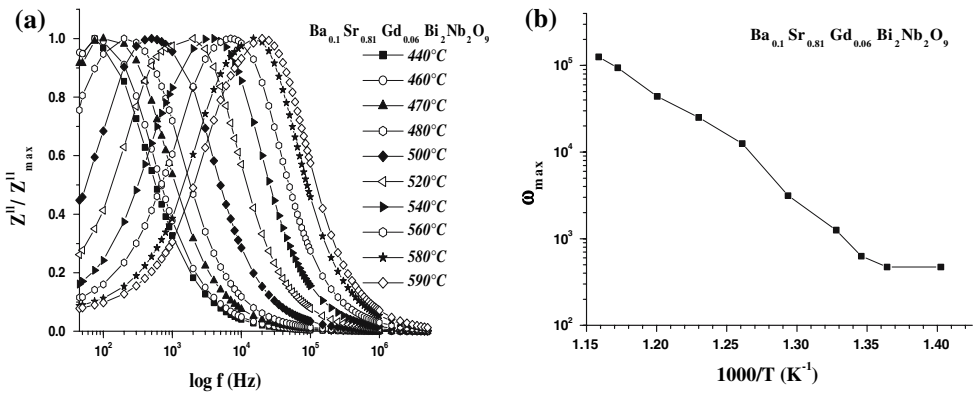


**Fig. 13** (**a**) Normalized imaginary parts, $Z''/Z''_{max}$, of the impedance as a function of frequency at several temperatures. (**b**) Variation of relaxational angular frequency with 1,000/$T$

where $\tau_m$ is the relaxation time. Figure 13b shows that the variation of relaxational angular frequency (i.e., frequency at which $Z''$ attains a peak at a particular temperature) with 1,000/T follows the Arrhenius law:

$$\omega_m = \omega_0 \exp(-E\tau/K_B T) \quad (10)$$

where $\omega_0$ is the pre-exponential factor. The activation energies have been calculated in the temperature regions 470–510 °C and 520–590 °C are 1.1 eV and 0.86 eV, respectively. These activation energies are close to that of oxygen vacancy motion, which is found to be in agreement with the earlier reports [70].

### *β Parameter*

The electric field relaxation due to ion motion is generally described by the Kohlrausch function $\phi(t) = \exp[-(t/\tau_\sigma)^\beta](0 \le \beta \le 1)$ [56–59], where $\tau_\sigma$ and $\beta$ are the conductivity relaxation time and Kohlrausch exponent, respectively. Smaller the value of $\beta$ the greater is the deviation with respect to Debye-type relaxation. The $\beta$ parameter is most often interpreted as a result of correlated motions between the ions. The value of $\beta$ becomes smaller as the cooperation between the charge carriers is more extended. For very small charge carriers concentration, the conductivity is essentially characterized by the independent jumps, where as when the mobile ion concentration increases, the coupling between charge carriers is more extended. In glasses and crystalline ionic conductors, the value of $\beta$ is close to 0.5 [59, 60].

The value of $\beta$ was determined by fitting the circular arc $Z^{II} = f(Z^I)$, the centre of semicircle displaced below the $x$-axis. The above fit allows us to determine the value of angle $\phi$ and thus $\beta$ as $\phi = (1 - \beta)\pi/2$. Variation of stretched exponential parameter, $\beta$ with temperature (440–590 °C) in BSGBN which covers $T_C$ of the material as shown in Fig. 14. From Fig. 14, at 590 °C the value of $\beta$ is approximately 0.97, it takes a minimum value about 0.84 at $T_C$, with further increase in temperature the $\beta$ value

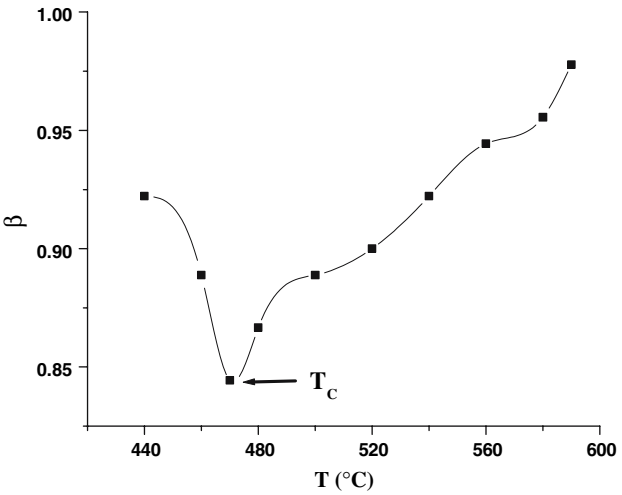


**Fig. 14** Variation of stretched exponential parameter, $\beta$ with temperature

increases in BSGBN. One can conclude, from the results that the variation of activation energy and stretched exponential parameter $\beta$ near $T_C$, the dynamic process is different from that of apart from phase transition temperature. According to lattice dynamics theory one of the transverse mode (soft mode) is weakened and the restoring force tends to become zero at ferroelectric–paraelectric transition [61]. Hence, if one assumes, that the charge carriers couples with soft mode, one may expect that the charge carriers become mobile at $T_C$.

### *Electric modulus characterization*

An alternative approach to investigate the electrical response of the materials is to use the complex electric modulus formalism [62], $M^*(\omega) = M' + jM''$. Electric modulus was introduced to study space charge relaxation phenomena, $M^*$ representation is now widely used to analyse ionic conductivities [63]. It can be represented by the following equation: $M^*(\omega) = j\omega C_0 Z^*(\omega) = 1/\varepsilon^*(\omega)$, where $j = \sqrt{-1}$ and $C_0$ is the vacuum capacitance of the

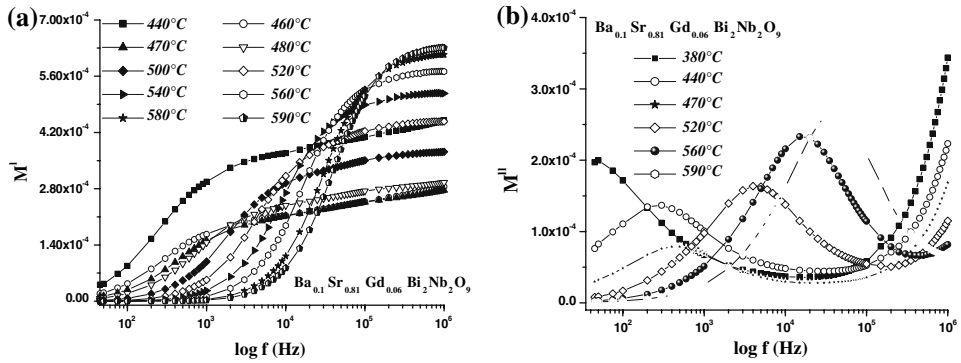


**Fig. 15** The real and imaginary parts of electric modulus, $M'$ and $M''$ as a function of frequency at various temperatures

cell, and is the complex permittivity. This formalism is particularly suitable to detect bulk phenomena properties as an average conductivity relaxation times [64].

The real and imaginary parts of electric modulus, $M'$ and $M''$ as a function of frequency at various temperatures have been depicted in Fig. 15. From Fig. 15a for each temperature, $M'$ reaches a constant value at higher frequencies. At low frequencies, $M'$ approaches zero, confirming the presence of an appreciable electrode and/or ionic polarization in the studies temperature ranges. The value of $M'$ increases from the low frequency of zero to a high-frequency limit $M_s$, and the dispersion shift to the high frequency as increase in temperature.

From Fig. 15b the peak appear in $M''$ at and above 380 °C shifts towards higher frequency side with increase in temperature. The magnitude of the peak decreases with increase in temperature as one approach the $T_C$, and again increases with increase in temperature. These peaks indicate the transition from short range to long range mobility with decreasing frequency, where the low-frequency side of the peak represents the range of frequencies in which the ions are capable of moving long distance, i.e., performing successful hopping from one site to the neighbouring site, whereas, for the high-frequency side, the ions are spatially confined to their potential wells and can execute only localized motion [65, 66].

The peak frequency is given by the relation $2\pi f_p \tau = 1$, is typically correlated with the average conductivity relaxation time. Figure 16 shows the Arrhenius pot of relaxational angular frequency $\omega_p = \omega_0 \exp[-E/kT]$. Where $\omega_o$ and T are the pre exponential of relaxational angular frequency and the absolute temperature respectively. Two distinct slopes of activation energies, above and below the $T_C$ of BSGBN obtained (Fig. 16) from Arrhenius plots and are tabulated in Table 4.

The representations of $Z''$ and M'' as a function of frequency at 470 °C is shown in Fig. 17. These representations of $Z''$ and $M''$ permit analysis of apparent polarization (space charge) by inspection of the magnitude of mismatch between the peaks of the both parameters. A significant mismatch was observed in $Z''$ and $M''$ peaks in the

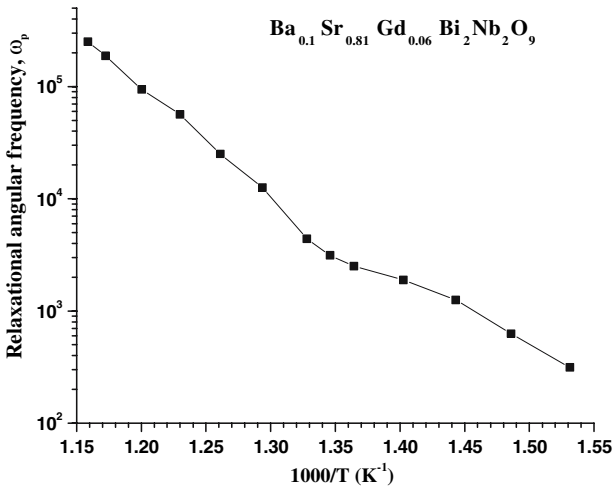


**Fig. 16** Arrhenius plot of relaxational angular frequency as a function of $1/T$

**Table 4** Activation energies of relaxation frequencies from $M''$ peaks as a function of $1/T$

| Temperature range (°C) | BSGBN dc conduction activation energies (eV) |
|---|---|
| 500–590 | 0.91 |
| 380–460 | 0.86 |

measured frequency range. This significant mismatch of $Z''$ and $M''$ peaks indicates the presence of Maxwell–Wagner type space charge polarization arising at defects (grain boundaries, sample–electrode interfaces) present in the sample. The frequency explicit plots of $Z''$ and $M''$ indicates departures from the ideal Debye behaviour. In ideal case the $Z''$ and $M''$ peaks should be coincident on the frequency scale [67].

## Conductivity

Thermal behaviour of dc ($\sigma_{dc}$) and ac conductivity ($\sigma_{ac}$) in BSGBN is shown in Fig. 18. It is observed from the plots

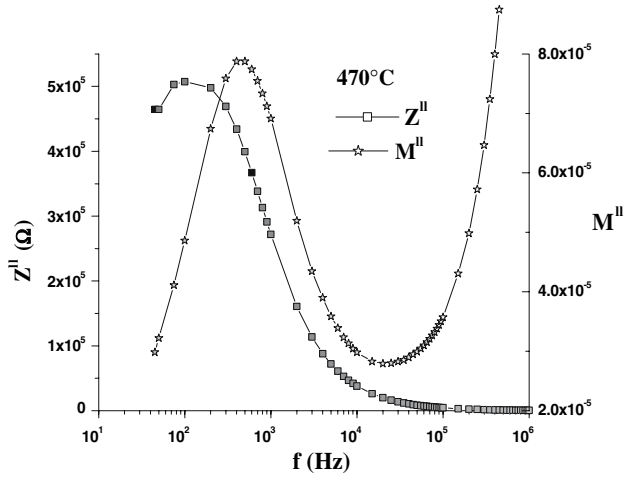


**Fig. 17** Representation of $Z''$ and $M''$ as a function of frequency at 470 °C

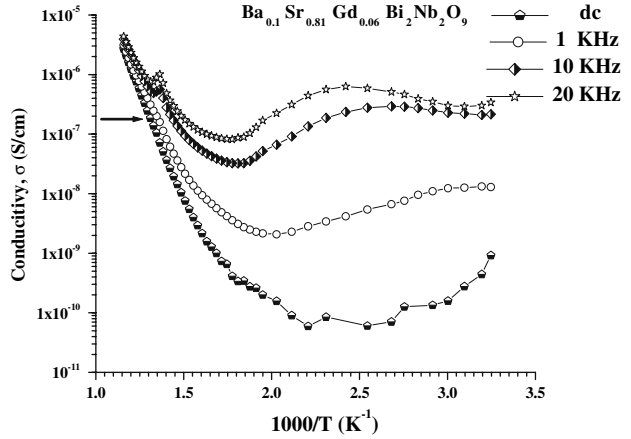


**Fig. 18** Thermal behaviour of dc ($\sigma_{dc}$) and ac conductivity ($\sigma_{ac}$) in BSGBN

that in low-temperature regime, the conductivity behaviour is observed to be dispersive [68]. With increase in temperature dispersion in conductivity narrowed and all the curves for different frequencies appeared to be merged into a single curve at high temperatures (>520 °C), indicting an onset of intrinsic conductivity mechanism that dominates at those temperature [69]. It has also been observed that the dc conductivity of the sample at lower temperature is deviating and magnitude is few orders less than that of the ac conductivity, and its variation at low temperature is also different. This may be due to the dc conductivity is determined by the most difficult transition in complete percolation paths between the electrodes, while the ac conductivity is determined by the easiest local movement of the charges.

The ac conductivity is drawn as a function of inverse of temperature, and ac conduction activation energy values in

**Table 5** Ac and Dc conductivity activation energy values in BSGBN

| Composition | BSGBN | | | |
|---|---|---|---|---|
| Temperature range (°C) | 20 KHz | 10 KHz | 1 KHz | dc |
| 300–390 | 0.09 | 0.08 | 0.21 | 0.27 |
| 400–460 | 0.20 | 0.41 | 1.12 | 1.38 |
| 500–590 | 0.52 | 0.52 | 0.85 | 0.83 |

BSGBN were calculated from the slope of Fig. 18 of Arrhenius plots, and the values are given in Table 5. The ac and dc conductivity activation energies in the ferroelectric region (400–460 °C) are 1.12 and 1.38, respectively, which may be ascribed to the motion of oxygen vacancies [70]. Oxygen vacancies are considered to be the most mobile charge carriers in layered pervoskite ferroelectric like SBN and SBT [71].

## Conclusions

Polycrystalline, $Ba_{0.1}Sr_{0.81}Gd_{0.06}Bi_2Nb_2O_9$ was indexed to be single phase with orthorhombic structure. The lattice parameters $a$ is slightly decreased and $c$ is increased by simultaneous substitution of $Ba^{2+}$ and $Gd^{3+}$ in SBN. Simultaneous substitution of $Ba^{2+}$ and $Gd^{3+}$ in SBN increased the $T_C$ to 470 °C from 392 °C. $T_C$ is found to be independent of frequency indicating the material BSGBN belongs to ferroelectric but not relaxor. From the impedance and modulus spectroscopic studies the material showed relaxation effects which are non-Debye type. The relaxation frequencies shifted to higher frequency side with increase in temperature. The bulk resistance calculated from Cole-Cole plot gives dc conductivity indicating that the conductivity mechanism is dominated by grain boundary conduction through hopping electrons created due to oxygen vacancies. Thermal behaviour of ac conductivity showed change in slope at $T_C$ and found to merge at higher temperatures due to onset of intrinsic conductivity.

## References

1. Aurivillius B (1949) Ark Kemi 1:463
2. Aurivillius B (1950) Ark Kemi 1:499
3. Aurivillius B (1950) Ark Kemi 2:519
4. Furusawa Y, Doi H (1999) Jpn J Appl Phys 38:6864
5. Cho CR (1999) Mater Sci Eng B Solid 64:113
6. Yoon SM, Tokimitsu E, Ishiwara H (1998) Jpn J Appl Phys 37:L396
7. Kim TY, Kim D, Chung CW (1997) Jpn J Appl Phys 36:6494
8. Wang F, Leppavouri S (1997) J Appl Phys 82:1293
9. Chen YC, Sun L, Yu T et al (1995) Thin Solid Films 269:18
10. De Araujo CAP, Cuchiaro JD, Mcmillan LD, Scott MC, Scott JF (1995) Nature 374:627

11. Majumder SB, Dobal PS, Bhaskar S, Katiyar RS (1999–2000) Ferroelectrics 241:287
12. Cheol-Hoon Y, Jae-Sun K, Soon-Gil Y (1998) Integ Ferro 21:475
13. Cheol-Hoon Y, Sang-Shik P, Soon-Gil Y (1997) Integ Ferro 18:377
14. Scott JF, De Araujo CAP (1989) Science 246:1400
15. Jimenez B et al (2000) J Phys Condens Matter 12:3883
16. Subba Rao EC (1962) J Am Ceram Soc 45:166
17. Zanetti SM et al (2000) J Mater Res 15:2091
18. Shibata K, Shoji K, Sakata K (2001) Jpn J Appl Phys 40:5719
19. Nanno M, Hirose M, Tsukada T (2001) Jpn J Appl Phys 40:5727
20. Subba Rao EC (1962) J Phys Chem Solids 23:665
21. Subba Rao EC (1961) J Chem Phys 34:695
22. Subba Rao EC (1961) Phys Rev 122:804
23. Newnham RE, Wolf RW, Horsey RS, Diaz-Colon FA, Kay MI (1973) Mater Res Bull 8:1183
24. Duran-Martin P, Castro A, Milan P, Jimenez B (1998) J Mater Res 13:2565
25. Millan P, Remirez A, Castro A (1995) J Mater Sci Lett 14:1657
26. Millam P, Castro A, Torrance TB (1993) Mater Res Bull 28:117
27. Atsuki T, Soyama N, Yonezawa T, Ogi K (1995) Jpn J Appl Phys 34:5096
28. Lu C, Wen C (1999) Mater Res Soc Symp Proc 541:229
29. Forbess MJ, Seraji S, Wu Y, Nguyen CP, Cao GZ (2000) Appl Phys Lett 76:2934
30. Desu SB, Vijay DP (1995) Mat Sci Eng B 32:83
31. Desu SB, Li T (1995) Mat Sci Eng B 34:L4
32. Kato K, Zheng C, Finder JM, Dey SK, Totti Y (1998) J Am Ceram Soc 81:1869
33. Desu SB, Vijay DP, Zhang X, He BP (1996) Appl Phys Lett 69:1719
34. Wu Y, Cao GZ (1999) Appl Phys Lett 75:2650
35. Wu Y, Cao GZ (2000) J Mater Sci Lett 15:267
36. Venkataraman BH, Varma KBR (2003) J Phys Chem Solids 64:2015
37. Venkataraman BH, Varma KBR (2005) Ferroelectrics 324:121
38. Aoyagi R, Takeda H, Okamura S, Shiosaki T (2005) Mat Sci Eng B 116:156
39. Wu E (1989) POWD, an interactive powder diffraction data interpretation and indexing program, version 2.1. School of Physical Sciences, Flinders University of South Australia, Bedford Park, SA 5042, Australia
40. Subba Rao EC (1962) J Am Ceram Soc 45:166
41. Watanabe H, Mihira T, Yoshimori H, De Araujo CAP (1995) Jpn J Appl Phys Part 1 34:5240
42. Liu J, Zou G, Yang H, Cui Q (1994) Solid State Commun 90(6):365
43. Zhigao L, Bonnet JP, Ravez J, Hagenmuller P (1992) Solid State Ionics 57:235
44. Nealon TA (1987) Ferroelectrics 76:377
45. Jonscher AK, Hill RM, Pickup C (1985) J Mater Sci 20:4431
46. Roling B, Happe A, Funke K, Ingram MD (1997) Phy Rev Lett 78:2160
47. Lee WK, Liu JF, Nowick AS (1991) Phy Rev Lett 67:1559
48. Lu Z, Bonnet JP, Ravez J, Hagenmuller P (1991) Eur J Solid State Inorg Chem 7(2):363
49. Jonscer AK (1983) Dielectric relaxation in solids. Chelsea Dielectric Press, London
50. Badwal SPS (1988) In: Proceedings of the international seminar on solid state ionic devices. World scientific publishing, Singapore, p 165
51. Macdonald JR (1987) Impedance spectroscopy. Wiely, New York
52. Sinclair DC, West AR (1989) J Appl Phys 66(8):3850
53. IDEM (1994) J Mater Sci 29:6061
54. Plocharski J, Wieczoreck W (1988) Solid State Ionics 28–30: 979
55. Jonscer AK (1977) Nature 267:673
56. Williams G, Watts DC (1970) Trans Faraday Soc 23:625
57. Nagai KL, Martin SW (1989) PhysRev B 40:10050
58. Howell FS, Bose RA, Macedo PB, Moynihan CT (1974) J PhysChem 78:639
59. Reqa JM, Rossignol S, Tanguy B, Paris MA, Rojo JM (1995) Snz J Solid State Ionics 80:283
60. Zouari N, Mnif M, Khemakhem H, Mhiri T, Daoud A (1998) Solid State Ionics 110:269
61. Zhigao L, Bonnet JP, Ravez J, Reau JM, Hagenmuller P (1992) Phys Chem Solids 53:1
62. Macedo PB, Moynihan CT, Bose R (1972) Phys Chem Glasses 13:171
63. Angell CA (1990) Chem Rev 90:523
64. Gerhardt R (1994) J Phys Chem Solids 55:1491
65. Kim JS (2001) J Phys Soc Jpn 70:3129
66. Liu J, Duan CG, Yin WG, Mei WN, Smith RW, Hardy JR (2003) J Chem Phys 119:2812
67. James AR, Priya S, Uchino K, Srinivas K (2001) J Appl Phys 90:3504
68. James AR (1997) Ph.D. Thesis, OU Hyderabad
69. Prasad NV, Prasad G, Bhimashankaram T, Suryanarayana SV, Kumar GS (2001) Int J Mod Phys B 15:2053
70. Chen TC, Thio CL, Desu SB (1997) J Mater Res 12(10):2628
71. Venkataraman BH, Varma KBR (2005) J Mater Sci Mater Electron 16(6):335